Materials Today Advances 23 (2024) 100511

Contents lists available at ScienceDirect

Materials Today Advances

journal homepage: www.sciencedirect.com/journal/materials-today-advances/

Interfacing two-dimensional and magnetic topological insulators: Bi bilayer on $MnBi_2Te_4$-family materials

I.I. Klimovskikh [a,*], S.V. Eremeev [b], D.A. Estyunin [c], S.O. Filnov [c], K. Shimada [d], V.A. Golyashov [e,c,m], N.Yu. Solovova [m], O.E. Tereshchenko [e,c,m], K.A. Kokh [f,c], A.S. Frolov [n,g], A.I. Sergeev [n,g], V.S. Stolyarov [n,a], V. Mikšić Trontl [h], L. Petaccia [i], G. Di Santo [i], M. Tallarida [j], J. Dai [j], S. Blanco-Canosa [a,k], T. Valla [a], A.M. Shikin [c], E.V. Chulkov [a,c,l]

[a] Donostia International Physics Center (DIPC), 20018 Donostia-San Sebastián, Basque Country, Spain
[b] Institute of Strength Physics and Materials Science, Russian Academy of Sciences, 634055 Tomsk, Russia
[c] Saint Petersburg State University, 198504 Saint Petersburg, Russia
[d] Research Institute for Synchrotron Radiation Science, Hiroshima University, Hiroshima, Japan
[e] Synchrotron Radiation Facility SKIF, Boreskov Institute of Catalysis, Siberian Branch, Russian Academy of Sciences, Kol'tsovo 630559, Russia
[f] Sobolev Institute of Geology and Mineralogy, Siberian Branch, Russian Academy of Sciences, 630090 Novosibirsk, Russia
[g] Lomonosov Moscow State University, Leninskie Gory 1/3, Moscow 119991, Russia
[h] Centre for Advanced Laser Techniques, Institute of Physics, 10000 Zagreb, Croatia
[i] Elettra Sincrotrone Trieste, Strada Statale 14 km 163.5, 34149 Trieste, Italy
[j] ALBA Synchrotron Light Source, Cerdanyola del Vallès, 08290 Barcelona, Spain
[k] IKERBASQUE, Basque Foundation for Science, 48013 Bilbao, Spain
[l] Departamento de Polímeros y Materiales Avanzados: Física, Química y Tecnología, Facultad de Ciencias Qumicas, Universidad del País Vasco UPV/EHU, 20080 San Sebastián/Donostia, Basque Country, Spain
[m] Novosibirsk State University, Novosibirsk, 630090, Russia
[n] Moscow Center for Advanced Studies, Kulakova str. 20, Moscow, 123592, Russia

ARTICLE INFO

Keywords:
Magnetic topological insulators
2D materials
Photoelectron spectroscopy

ABSTRACT

Meeting of non-trivial topology with magnetism results in novel phases of matter, such as quantum anomalous Hall (QAH) or axion insulator phases. Even more exotic states with high and tunable Chern numbers are expected at the contact of intrinsic magnetic topological insulators (IMTIs) and 2D topological insulators (TIs). Here we synthesize a heterostructures composed of 2D TI and 3D IMTIs, specifically of bismuth bilayer on top of $MnBi_2Te_4$-family of compounds and study their electronic properties by means of angle-resolved photoelectron spectroscopy (ARPES) and density functional theory (DFT). The epitaxial interface is characterized by hybridized Bi and IMTI electronic states. The Bi bilayer-derived states on different members of $MnBi_2Te_4$-family of materials are similar, except in the region of mixing with the topological surface states of the substrate. In that region, the new, substrate dependent interface Dirac state is observed. Our *ab initio* calculations show rich interface phases with emergence of exchange split 1D edge states, making the Bi/IMTI heterostructures promising playground for observation of novel members in the family of quantum Hall effects.

1. Introduction

Discovery of intrinsic magnetic topological insulators (IMTIs) boosts the research on quantum anomalous Hall (QAH) effect and axion electrodynamics and gives a new hope for Majorana zero modes observation [1–13]. The QAH phase is characterized by non-zero Chern number ($C = 1$), topologically protected chiral edge states and quantized Hall conductance at zero magnetic field [14–16]. The most studied IMTI compound, $MnBi_2Te_4$ (MBT), is a layered van-der-Waals crystal [1,17,18]. Predicted antiferromagnetic interlayer ordering had been confirmed experimentally, as well as the exchange interaction impact on the topological band structure, fulfilling the requirements for QAH effect observation [19].

Apart from the QAH with $C = 1$, it is possible to realize the topological materials with higher and tunable Chern numbers whose multiple dissipationless edge conduction channels could significantly improve the performance of quantum devices [20–24]. Recently such a tunable high-Chern number phase has been predicted for the interface

* Corresponding author.
E-mail address: ilya.klimovskikh@dipc.org (I.I. Klimovskikh).

https://doi.org/10.1016/j.mtadv.2024.100511
Received 27 April 2024; Received in revised form 21 June 2024; Accepted 21 June 2024
Available online 13 July 2024

of 2D topological insulators and $MnBi_2Te_4$ [25,26]. As an exciting example in Ref. [25] authors theoretically demonstrate the multiple topological edge states and switchable Chern number ($C = \pm1, \pm3$) for the contact of bismuth bilayer with a single septuple layer of MBT.

Ultrathin bismuth films represent one of the most promising 2D topological materials, whose unique properties had been successfully demonstrated in various structures, such as bismuthene and Bi(110) or Bi(111) films [27–33]. Recently ferroelectric properties had been found for bismuth monolayer [34], that opens a route for multiferroic features in two dimensions [35,36]. Due to the large spin–orbit interaction, the band gap in 2D bismuth is inverted, resulting in quantum spin Hall (QSH) phase and 1D spin-polarized states emerge at the edges of bismuth layer islands [32,37–39]. Experimentally, the most accessible form is Bi(111) bilayer. Its topological properties strongly depend on the interaction with the substrate [29,37,38]. Due to a good lattice match, materials like Bi_2Te_3 and other 3D TIs are generally suitable substrates for Bi bilayer films. Interestingly, the interaction of the topological surface states of the substrate with Bi-related bands does not destroy the QSH phase and 1D-edge channels, as demonstrated in Refs. [39–41]. Depending on the interaction with the substrate, the contact of Bi bilayer with IMTI may also show other, yet undetected types of quantum Hall effect, such as time-reversal symmetry broken QSH [42–46].

In this study we synthesize the heterostructures consisting of Bi-bilayer and magnetic topological insulators of the $MnBi_2Te_4$ family. By means of photoelectron spectroscopy (PES) and low energy electron diffraction (LEED) the epitaxial growth mode is confirmed, and electronic structure of the interfaces is studied by means of ARPES. Although the interaction between Bi-BL and IMTI surfaces is relatively weak, the topological surface states mix with the Bi-BL states, resulting in a specific interface electronic structure, supported by DFT calculations. Resulting band structure of the Bi-BL exhibits distinctive set of hole-like states, which weakly depend on the substrate composition. On the other hand, the interface Dirac cone-like feature around the $\bar{\Gamma}$ point is formed only for IMTI substrates with well-pronounced topological surface states within the bulk band gap. Furthermore, *ab initio* calculations predict the emergence of the 1D topological states at the edges of Bi-BL, that are exchange split due to interaction with the magnetic substrate.

2. Results

2.1. Bi bilayer on $MnBi_2Te_4$

Bulk $MnBi_2Te_4$ material consists of septuple layer blocks Te-Bi-Te-Mn-Te-Bi-Te, that stack together forming van der Waals (vdW) crystal. Therefore, cleavage of bulk $MnBi_2Te_4$ crystal in ultra-high vacuum (UHV) results in formation of atomically clean Te-terminated (0001) surface. In-plane lattice constant of 4.33 Å in $MnBi_2Te_4$ is almost the same as in Bi_2Te_3 (4.38 Å) and close to the one in Bi(111) (4.54 Å). Hence, it can be expected that deposition of Bi on top of $MnBi_2Te_4$ would lead to epitaxial growth of Bi(111) overlayers, similarly to Bi-bilayer on Bi_2Te_3 case [41,47,48]. Therefore, in order to fabricate and characterize the Bi bilayer on MBT we have deposited the corresponding amount of Bi on freshly cleaved MBT surface, slightly annealed it and carried out LEED and PES measurements to test the structural properties of the film and then performed the ARPES studies.

PES spectra of Bi 5*d* lines for MBT surface before and after bismuth deposition are presented in Fig. 1(a). Binding energies (BEs) of Bi $5d_{5/2,\ 3/2}$ peaks are 24.6 and 27.7 eV respectively, in accordance with previous works [50–53]. Deposition of Bi atoms results in a small shift of Bi 4*d* line by 0.2 eV towards the lower binding energies. Besides the slight change of the main peaks positions Bi 5*d* spectrum exhibits the appearance of additional peaks (violet color), with the BEs of 23.7 and 26.8 eV. The binding energy of these additional components corresponds to one Bi-bilayer, as shown in Refs. [54–56]. Taking into account the exponential decay of the photoelectron signal in depth the effective thickness of the Bi film can be estimated as $d = \lambda * ln(1 + 2/7 * I_{Bi_2}/I_{MBT})$, where λ is the mean free path of the photoelectron with a given kinetic energy and I_{Bi_2}/I_{MBT} is ratio of the intensities of Bi-BL and substrate contributions. Using this formula we obtain the effective thickness of ≈ 4 Å, that corresponds to a coverage of one bismuth bilayer (Bi-BL height is 3.8 Å). LEED data clearly demonstrate the 1 × 1 structure of the Bi overlayer on MBT, similar as in case of Bi_2Te_3 substrate.

In order to have a look into the band structure of the synthesized interface we have measured angle-resolved photoelectron spectra. ARPES images in a wide energy region before and after bismuth deposition are shown in Fig. 1b and c, respectively. Spectrum of pristine MBT surface consists of the set of strongly dispersive valence band states and parabolic conduction band near the Fermi level. Within the bulk band gap there are topological surface states, but their photoemission cross section strongly depends on the photon energy (see Ref. [57]), and at the used photon energy of 21.2 eV TSS are difficult to see. Formation of Bi-bilayer on top of MBT results in noticeable changes in the electronic spectra. First, valence band states shift towards the Fermi level by 0.1 eV, similarly to core levels shift, that is caused by the changes of the surface conditions. Moreover, one can see three new hole-like states in the ARPES spectrum, marked as α, β and γ. Two of these states (α and β) disperse up to 0.3 eV of BE at the $\bar{\Gamma}$-point, while the third one (γ) approaches the Fermi level. Similar band structure of Bi-bilayer had been observed on various substrates [27,39–41]. The Frank-Van der Merwe Bi film growth mechanism can be easily seen from the ARPES data for various Bi coverages, see Fig. S1 in Supplementary Information.

It is known that the electronic structure of free-standing Bi-bilayer is characterized by two degenerate hole-like valence states and electron-like conduction band [41]. Giant spin–orbit interaction results in the inversion of the gap between the valence and conduction bands, that turns Bi-bilayer to 2D QSHE topological insulator phase [38]. Growth of Bi-bilayer on the substrate leads to lifting of the inversion symmetry and the appearance of large Rashba-like splitting of the states [39–41,48]. Furthermore, Bi-BL and substrate surface states may hybridize, forming a novel 2D interface electronic system with peculiar topological properties [27,39–41]. Effects of electronic states hybridization in our Bi-BL/MBT system can be analyzed in zoomed region ARPES images, presented in Figs. 1d–g.

Spectrum of pristine MBT surface (Fig. 1d), taken at a photon energy of 28 eV exhibits the sharp gapped Dirac cone, formed by topological surface states. The Dirac point gap is of several tens meV, within the limits of previously reported values, ranging from zero to 80–90 meV [9,58]. As noted above, deposition of Bi-bilayer modifies the band structure, introducing several new hole-like Bi-related states, see Fig. 1e. In order to resolve this complicated dispersion relations we have calculated DFT band structure. Calculated spectrum along $\bar{\Gamma} - \bar{K}$ with projected weights from Bi-BL atoms imposed over the ARPES in Fig. 1e. One can see the pronounced Dirac cone-like feature around the $\bar{\Gamma}$-point, interacting with the hole Bi-related bands. The upper part of the Dirac cone mixes with the band γ, that is actually split (γ and γ'), with the value of the splitting being dependent on the wave vector, see intensity curvature plot in Fig. 1g. Similar splitting had been shown for Bi-BL on Bi_2Te_3 [41], and attributed to Rashba-like behavior due to inversion symmetry breaking. In the region of lower part of the Dirac cone-like state one can see two hole-like states (α and β), split by 0.2 eV in energy. The trigonal symmetry of photoemission intensity is seen at the constant energy cuts in Fig. 1f. Exchange interaction affects the Bi-BL/MBT interface states, that we study theoretically and will discuss below.

2.2. Bi bilayer on $MnBi_2Te_4$-family materials

Electronic and magnetic structure of MBT-family compounds can be tuned in two ways: by means of doping and superlattices formation.

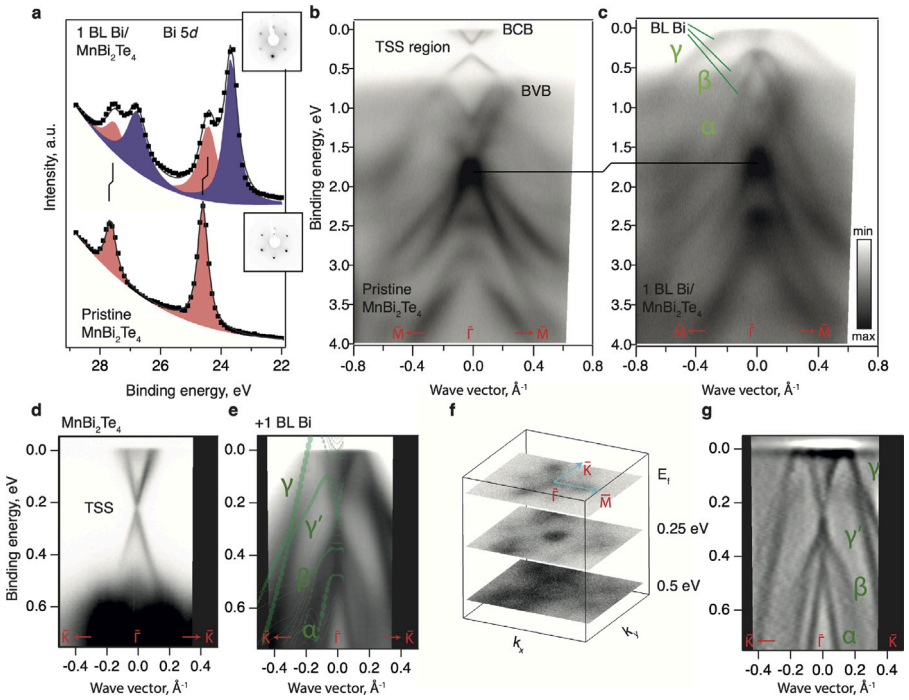

Fig. 1. (a) Experimental core level spectra and fitting data of Bi-5*d* lines for $MnBi_2Te_4$ before (lower spectrum) and after (upper spectrum) Bi-bilayer deposition. Data were taken at a photon energy of 40 eV. Upper and lower insets show corresponding LEED images taken at the primary electron energy of 80 eV. (b, c) ARPES dispersion relations in the wide energy region in the $\bar{\Gamma}\bar{M}$ direction of BZ of $MnBi_2Te_4$ taken at temperature of 76 K and at a photon energy of 21.2 eV before (b) and after (c) Bi deposition. (d,e) ARPES dispersion relations in the low energy region in the $\bar{K}-\bar{\Gamma}-\bar{K}$ direction of BZ of $MnBi_2Te_4$ taken at 17 K before (photon energy of 28 eV) (d) and after (photon energy of 20 eV) (e) Bi deposition. DFT calculated spectrum (green) is imposed on the left side of panel (e). (f) Constant energy maps in the $k_{\parallel}$-space taken at various binding energies. (g) Curvature plot (the procedure is described in Ref. [49]) of the ARPES data at (e). (For interpretation of the references to color in this figure legend, the reader is referred to the web version of this article.)

Doping by Pb,Sn or Ge atoms leads to closing of the bulk band gap at some point, forcing the system to become a Dirac semimetal [59–61]. Further doping leads to reopening of the bulk band gap, but such a system is not trivial and can be rather classified as dilute magnetic topological insulator [59]. On the other hand, exchange interaction and topological properties of MBT can be varied via superlattice $(MnBi_2Te_4)(Bi_2Te_3)_m$ formation, where m=0..6 [17].

We have synthesized Bi bilayer film on top of several MBT-family substrates, namely $Ge_{0.4}Mn_{0.6}Bi_2Te_4$, $MnBi_6Te_{10}$ and $Pb_{0.8}Mn_{0.2}Bi_4Te_7$ and novel $In_{0.25}Mn_{0.75}Bi_2Te_4$. Notably, doping and/or superlatticing for these compounds leads to decrease of the Néel temperature down to 12–15 K. The in-plane lattice constant and surface atomic structure of the compounds are very similar to MBT, and the growth mode of Bi-BL is also epitaxial, with 1×1 structure. Experimental dispersion relations of the electronic states for pristine surfaces and after Bi-BL adsorption on top are shown in Fig. 2.

The first panel (Fig. 2a) presents the ARPES data for $In_{0.25}Mn_{0.75}Bi_2Te_4$ material, where we can see the large bulk band gap (of around 350 meV), and no topological surface states within the gap. Thus, one can assume that In doping changes electronic structure of MBT significantly, resulting in trivial insulator phase. There is some diffuse intensity inside the gap, that can rather be attributed to impurity states or complex scattering processes. Deposition of Bi bilayer on top (Fig. 2e) leads to appearance of the hole like bands. The first, γ one, crosses the Fermi level at ≈ 0.2 Å^{-1}, similar to the γ band in Fig. 1 in the Bi-BL/MBT spectrum. One can also see the second hole-like state, that reaches 0.4 eV at $\bar{\Gamma}$ point and can be related to the β state, mixed with valence band of the substrate. Notably, in contrast to Bi-BL on MBT substrate there is no Dirac cone-like feature around the $\bar{\Gamma}$ point.

The second panel (Fig. 2b) shows the spectrum of $Ge_{0.4}Mn_{0.6}Bi_2Te_4$, characterized by a vanishing bulk band gap, making this system a magnetic Dirac semimetal [59]. One can see the valence and conduction band touching at the BE of around 0.2 eV. Bismuth bilayer deposition on top (Fig. 2f) of this substrate results in a pair of hole-like bands formation, shifted by 0.1 eV towards the higher BE, in comparison to Bi-BL on MBT and $In_{0.25}Mn_{0.75}Bi_2Te_4$. Rashba-split γ state has large intensity at the $\bar{\Gamma}$ point where the Kramers degeneracy takes place. Remarkably, the Dirac cone-like features are not visible, similar to Bi-BL on $In_{0.25}Mn_{0.75}Bi_2Te_4$. We suppose that the lack of the α state, that originates from mixing of the Bi-BL bands with the TSS and valence band states, can be related to weaker hybridization in the case of In and Ge-doped MBT substrates.

The last two panels of Fig. 2 show the electronic structure of pristine $MnBi_6Te_{10}$ (c) and $Pb_{0.8}Mn_{0.2}Bi_4Te_7$ (d) compounds, which are magnetic topological insulators with reduced exchange interaction, in comparison to MBT [17,61]. The crystal structure of these compounds can be viewed as alternating $MnBi_2Te_4$ septuple layer (SL) (without or with Pb alloying) and Bi_2Te_3 quintuple layer (QL) blocks, and cleaved surface consists of distinct SL or QL terminations, resulting in multiple Dirac cones structure in ARPES image. Bismuth bilayer on top of these two materials exhibits similar features, namely formation of hole-like α, β and γ bands, only with the difference in energy, being by 0.2 eV shifted to higher BE for $Pb_{0.8}Mn_{0.2}Bi_4Te_7$ substrate. Moreover, one can clearly see the Dirac cone feature in both cases, that is composed of substrate TSS and Bi-BL-related states, similarly to Bi-BL on MBT and Bi_2Te_3 substrates. We have to note that exchange interaction between the MBT blocks is significantly reduced for the systems of $(MnBi_2Te_4)(Bi_2Te_3)_m$-type, and for large m number the topmost MBT block can be viewed as almost non-interacting 2D ferromagnet. Contact of Bi BL with this termination on the surface may be of special interest for tunable Chern number properties [25].

Thus, the Bi bilayer exhibits similar set of hole-like bands for all studied MBT-family substrates, but interfacial Dirac cone-like feature is formed only if TSS are present in the bulk band gap of the topological substrate. These observations are in accordance with our theoretical simulations of Bi BL on MBT substrate, see the results below and in Supplementary Information.

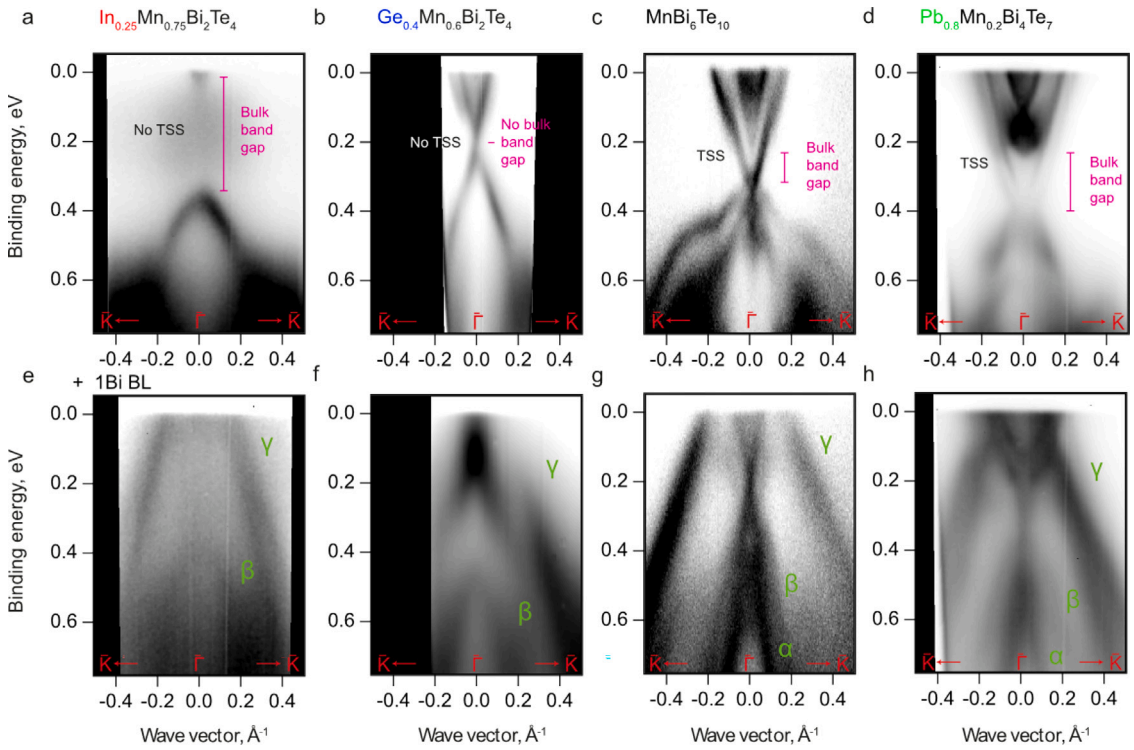

Fig. 2. ARPES dispersion relations in the low energy region in the $\bar{K} - \bar{\Gamma} - \bar{K}$ direction of BZ of $MnBi_2Te_4$-family samples taken at 17 K before (upper panels) and after (lower panels) Bi deposition. The photon energies are 20 eV for (a, d, e, f, h), 9 eV for (b), 30 eV for (c,g).

2.3. DFT calculations

To clarify the interaction of the deposited Bi-BL with MBT substrate and reveal how the formation of the interface affects the electronic structure of the Bi-BL we performed DFT calculations. Firstly, we have to note the preferred out-of-plane direction of the magnetic moments for Bi-BL/MBT system. This is in contrast to recently proposed vdW heterostructure composed of single $MnBi_2Te_4$ SL and Bi-BL [25], where the calculated magnetic easy axis is predicted to be in-plane, with a magnetic anisotropy energy (MAE) of $E_x - E_z = -0.15$ meV/Mn that is different from the out-of-plane magnetic easy axis of the free-standing $MnBi_2Te_4$ SL where MAE is +0.125 meV/Mn [62]. For our structure with thick $MnBi_2Te_4$ substrate we check the possibility to change the spin alignment in the outermost $MnBi_2Te_4$ SL due to Bi-BL interface formation. We found that total energy of the structure where magnetic moments of Mn atoms in the interfacial SL are placed in-plane is 0.07 meV/Mn less favorable compared to the case when the intrinsic out-of-plane magnetization of $MnBi_2Te_4$ is preserved, although this value is smaller than MAE in the free-standing SL.

2.3.1. Bi-BL/MBT surface electronic structure

The equilibrium structure of Bi-BL on the MBT surface is shown in Fig. 3a. The optimized interface distance between Bi-BL and topmost Te atomic layer of the MBT substrate is 2.52 Å, which is comparable to the vdW spacings in MBT bulk (2.53 Å) [1,63]. Our calculations for interactions between Bi and Te atoms at the Bi-BL/MBT interface and those (Te-Te) at the vdW spacing in the MBT, based on the projected crystal orbital Hamilton population method [64–66] show that the former one is only by factor 1.6 stronger (0.49 vs. 0.30 eV). Thus, the interaction between $MnBi_2Te_4$ surface and Bi-BL is close to the vdW type. At that, the charge transfer from Bi-BL to the substrate is negligibly small: it is only 0.14 e from the interfacial Bi layer and completely absent in the upper Bi layer. Such a small charge transfer is reflected in minor variation in the interface potential: $\Delta V(z)$ obtained as a difference between the electrostatic potentials within Bi-BL/MBT heterostructure and free-standing MBT (BL) does not exceed 20 meV in both MBT surface and Bi-BL film (Fig. 3b).

When the distance between Bi-BL and the surface is enlarged twice, up to 5 Å, Fig. 3c, one can clearly see the Bi-BL bands which lie a bit higher than in the spectrum of the free-standing Bi-BL (blue dashed lines). These bands demonstrate moderate Rashba-type splitting due to the inversion symmetry breaking. The gapped topological surface state of the MBT surface is also present in the spectrum. Despite the practically absent interaction between the bilayer and the surface in this case the TSS hybridizes with upper and second valence bands of the Bi-BL with the formation of small hybridization gaps at the Fermi level and at ≈ -0.15 eV, respectively. In contrast, at equilibrium interface distance (Fig. 3d) the spectrum of the heterostructure undergoes significant changes, becoming strongly $\bar{\Gamma} - \bar{K}/\bar{\Gamma} - \bar{M}$ anisotropic and demonstrating mixed BL/SL localization of the surface states within MBT bulk gap. Such a behavior is typical for the TSSs which tend to penetrate into the overlayer [67]. This effect is observed on both nonmagnetic [68,69] and magnetic [70] TIs and also underlies the formation of magnetic extension heterostructures [2,71,72]. As can be seen in Figs. 3e,f all surface states in the Bi-BL/MBT heterostructure locating mostly in the Bi-BL overlayer penetrate deep into the MBT substrate down to the second SL. Owing to their predominant localization in the Bi bilayer, these states generally inherit the dispersion of the Bi-BL and are similar to the states in the heterostructure formed by Bi-BL on a nonmagnetic TI [39], but due to their penetration into the magnetic substrate, the $\bar{\Gamma}$ degeneracies are lifted, with the value of exchange splitting of around 10 meV. Another effect of magnetic substrate on the surface states arising from hybridization of the Dirac state of MBT and Rashba state of Bi-BL is appearance of $\bar{\Gamma} - \pm\bar{K}$ asymmetry (Fig. 3e), similar to that in the Dirac state of $MnBi_2Te_4$ [1]. This asymmetry, is absent along $\bar{\Gamma} - \bar{M}$ where the mirror plane symmetry obliges the out-of-plane spin components to be zero for both Rashba and Dirac states. However, for the $\bar{\Gamma} - \bar{K}$ directions the nonzero S_z components are allowed by symmetry and they coexist with the in-plane spin components. Since the surface states do not penetrate deeper than the topmost SL, where

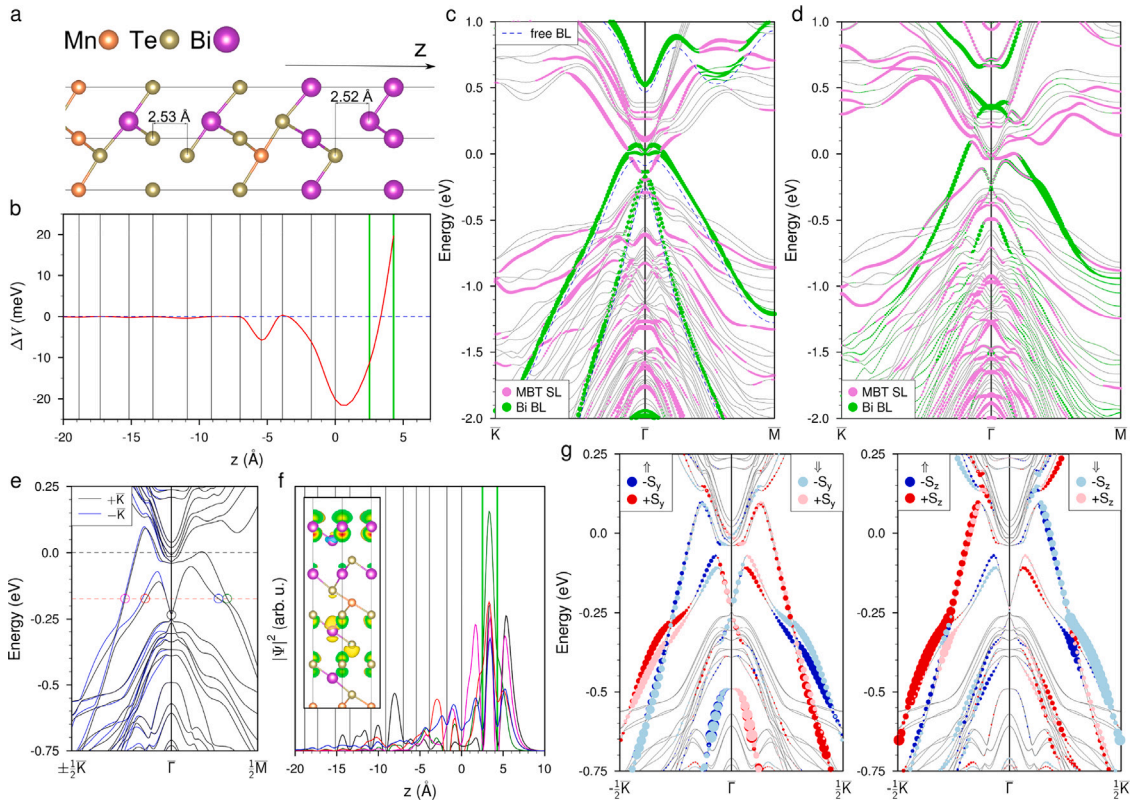

Fig. 3. (a) Equilibrium atomic structure of Bi-BL/MBT. (b) The interface potential obtained as a difference between the integrated over xy plane $V(z)$ potentials within Bi-BL/MBT heterostructure and free-standing MBT(BL) slab: $\Delta V(z) = V_{\mathrm{Bi-BL/MBT}} - V_{\mathrm{MBT(BL)}}$. (c) Calculated band structure of Bi-BL/MBT heterostructure when the distance between Bi-BL and MBT surface is twice as large with respect to the equilibrium one. Dashed blue curves show the spectrum of freestanding Bi-BL; size of green and violet dots denote weights of the states localized in the Bi-BL and outermost SL of MBT, respectively. (d) The same as in the panel (c) but for equilibrium position of the Bi-BL. (e) Magnified view of the spectrum shown in panel (d) in the vicinity of the bulk gap of MBT. $\pm\bar{K}$ curves correspond to dispersion of the states along nonequivalent for magnetic $MnBi_2Te_4$ $\bar{\Gamma}-\bar{K}$ and $\bar{\Gamma}-{-}\bar{K}$ directions, respectively. Color circles show states for which the spatial distribution is presented in panel (f) with the same colors. (f) Integrated over xy spatial distributions of the states marked in panel (e). Inset show the charge density of the $\bar{\Gamma}$ state (black line). (g) Spin texture of the surface states in the Bi-BL/MBT heterostructure along the $-\bar{K}-\bar{\Gamma}-\bar{K}$ direction with in-plane (S_y, left side) and out-of-plane (S_z, right side) components. Dark and light red/blue circles show positive/negative components for different magnetization orientation in the topmost $MnBi_2Te_4$ SL: along (⇑) and against (⇓) the surface normal, respectively. (For interpretation of the references to color in this figure legend, the reader is referred to the web version of this article.)

Mn magnetic moments are ferromagnetically ordered, the $\bar{\Gamma}-{+}\bar{K}$ and $\bar{\Gamma}-{-}\bar{K}$ branches with nonzero S_z interact differently with the Zeeman field provided by the Mn layer of the topmost SL block and this interaction and resulting alteration in the $\bar{\Gamma}-\pm\bar{K}$ dispersions depends on the magnetization direction in the topmost SL (Fig. 3g). Notably, similarly to pristine MBT case, this asymmetry is difficult to observe experimentally, since magnetic domains with opposite orientation of the Mn magnetic moments are always present on the surface, and ARPES measures the average signal from both types of domains.

2.3.2. Bi-BL edge electronic structure on flat and stepped MBT surfaces

Further, we have calculated the electronic structure of Bi-bilayer nanoribbon on top of MBT, in order to analyze whether quantum spin Hall phase of Bi-BL survives or not. For this end we constructed the $1 \times 7\sqrt{3}$ MBT supercell with zig-zag edged Bi-BL ribbon on the top surface (Fig. 4a). In this supercell in the AFM MBT slab the Mn magnetic moments in the topmost SL were pointed outward the surface plane. The calculated edge spectrum of the freestanding Bi-BL ribbon (Fig. 4b, dashed blue curves) agrees well with earlier work [73]. Note that the calculations of Bi-BL ribbon on nonmagnetic TI [39] revealed that overall band dispersion, the Dirac cone at the zone boundary and the helical spin texture of the edge states are preserved and consistent qualitatively with that of a free-standing Bi(111) BL despite of strong hybridization of the Bi-BL bands with the substrate. As can be seen in the Fig. 4b the dispersion of the topological edge states of Bi-BL on MBT AFMTI also survives far from the BZ center in which the states fall into 2D continuum of the hybridized Bi-BL/MBT states crossing the MBT bulk gap (green area in Fig. 4b). The difference from the spectrum of free-standing bilayer is that the spectra of left and right zig-zag edges, which were degenerate in the free BL, are different on the MBT substrate due to different atomic relaxation of the opposite edges and different spatial localization of the edge states. Note that the similar behavior is observed for the Bi bilayer on other substrates and the edges are usually called as A- and B-type edges [28] (Fig. 4a). The state localized on the left (B-type) edge having maximum charge localization on the most extreme atoms of the BL ribbon rapidly penetrates deep into the topmost SL while on the opposite (A-type) edge the 1D state propagates within the BL and only partially penetrates into the substrate. This penetration of the edge states into magnetic substrate results in opening of the gaps in the Dirac states at the BZ boundaries. The exchange gap in Dirac point of the A-type edge state amounts 36 meV while it is much larger, of 82 meV, for the B-type edge state, which penetrates well to the manganese layer. Similarly to $\bar{\Gamma}-\pm\bar{K}$ asymmetry in the 2D spectrum of the Bi-BL/MBT the Bi-BL edge spectrum also demonstrate $\bar{\Gamma}-\pm\bar{X}$ asymmetry (note that 1D BZ direction coincides with the $-\bar{K}-\bar{\Gamma}-\bar{K}$ direction the 2D BZ, see top inset in Fig. 4b). This asymmetry stem from interaction of the spin-polarized edge states demonstrating considerable S_z spin component (bottom inset in Fig. 4b) and Zeeman field of the topmost SL. It is evident that the presented in Fig. 4b dispersion of the edge states along $-\bar{X}-\bar{\Gamma}-\bar{X}$ will be reversed when the direction of the Mn magnetic moments in the topmost SL will be opposite.

It is known the MBT surfaces usually contain steps of SL height and change in the direction of the surface layer magnetization in

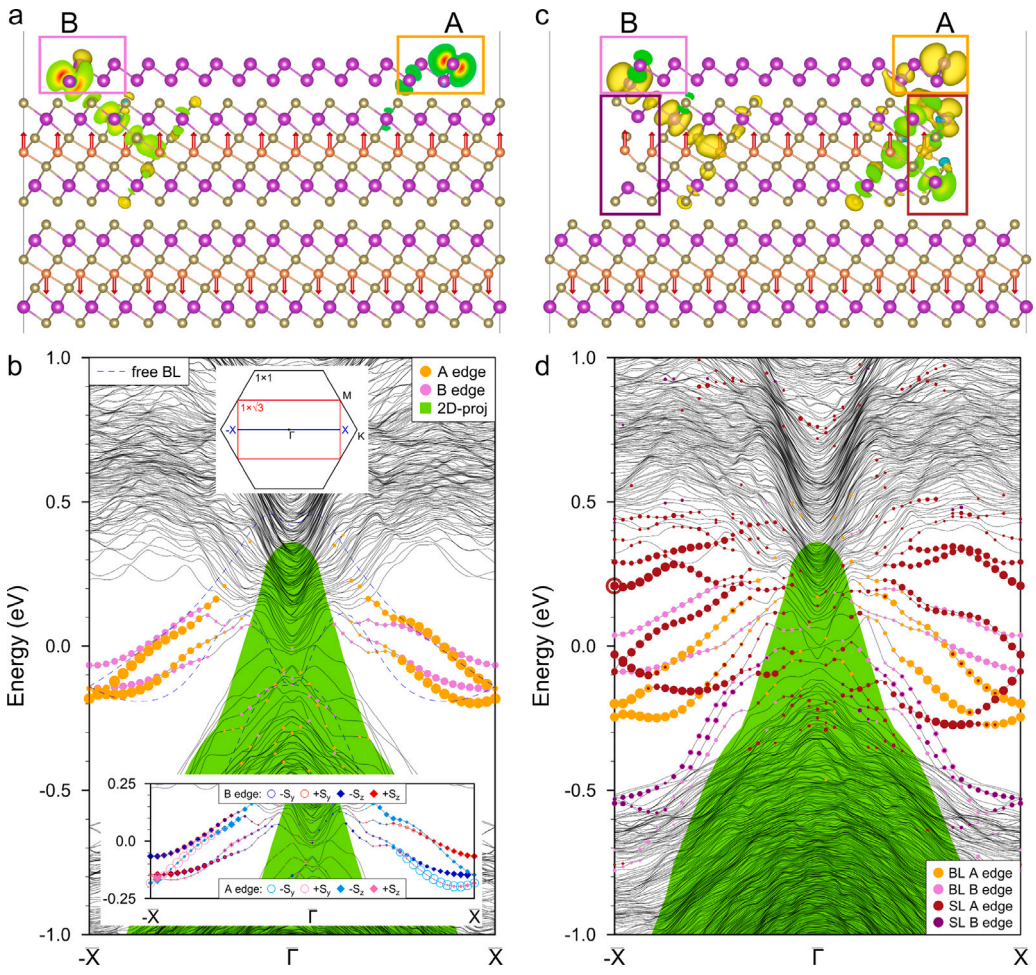

Fig. 4. (a) Side view of the atomic structure of $1 \times 7\sqrt{3}$ $MnBi_2Te_4$ surface supercell with Bi-BL ribbon ontop and spacial charge distribution of the 1D states localized on right (A-type) and left (B-type) ribbon edges. Colored boxes show the areas over which the atomic weights of the states (shown in panel (b) in the same colors) were collected. Red arrows show Mn magnetic moments. (b) Edge band structure of Bi-BL ribbon on flat $MnBi_2Te_4$ surface calculated along $-\bar{X} - \bar{\Gamma} - \bar{X}$ direction of the 1D BZ (see top inset). Green area depicts projection of 2D states (hybridized Bi-BL/MBT states), crossing the MBT bulk gap, onto 1D BZ. Orange and violet circles show weights of the 1D states localized on A and B edges of the ribbon, respectively. Dashed blue curves show the spectrum of zig-zag edge states in the freestanding Bi-BL ribbon. Bottom inset demonstrate spin texture of the edge states. (c and d) The same as in panels (a,b) but in this case the Bi-BL ribbon is connected with a step on the MBT surface. Weights of the states localized on Bi-BL and MBT-SL edges are shown separately with colors pointed in the key. (For interpretation of the references to color in this figure legend, the reader is referred to the web version of this article.)

MBT AFMTI is related to these steps [74]. Despite the terraces are usually wide and step density is relatively small we also consider the Bi bilayer edge coinciding with the step edge on the MBT substrate in order to find out whether the edge states of the Bi bilayer survive in such a geometry. Besides, in the recently proposed free-standing vdW heterostructure composed of single $MnBi_2Te_4$ SL and Bi-BL [25] in case of out-of-plane magnetization within SL the TB calculations predict the emergence of topologically protected edge states. In our model the constructed ribbon composed of Bi-BL and MBT SL (Fig. 4c) presents such a heterostructure, however, forming in a natural way at the edge of the step and supported by MBT bulk. The results show (Fig. 4d) that MBT gap region possess a plenty of the states originating from the dangling bonds of the SL edges (the spatial localization only one of them, marked with open brown circle in the panel d is shown in the panel c). In addition to these states in the spectrum, one can easily find out the states of the Bi-BL edges (violet and orange circles in panel d). In this case, the dispersion of A-type edge state on the whole is shifted lower in energy compared to the Bi-BL on the flat terrace while that of the B-type edge is shifted up so that the upper branch becomes completely unoccupied. Besides, the $\pm\bar{X}$ Dirac point exchange gaps are enlarged for both B-type and A-type edge states, up to 122 and 46 meV, respectively, which should indicate an increased overlap of the edge states with the manganese layer, although in general the spatial distribution of the edge states (Fig. 4c) looks similar to that on the flat terrace. It is also worth noting that the $\bar{\Gamma} - \pm\bar{X}$ asymmetry, controlled by the direction of magnetization in the upper Mn layer is preserved in this case as well.

It should also be noted that STM topographic measurements of $MnBi_2Te_4$ surface show that the edges of the SL steps have a more complex and variable geometry [75] than the edges used in our simulation, which are strictly perpendicular to the surface, and hence the dispersion of the states localized on the SL edges in real samples will differ from obtained in the calculation.

3. Conslusions

In summary, we have fabricated and studied a number of heterostructures composed of Bi bilayer and $MnBi_2Te_4$-family materials. Similar lattice constants of Bi(111) and IMTI compounds results in epitaxial growth mode and 1 × 1 structure of the Bi film. Electronic states of Bi-BL and IMTI hybridize, forming a joint interface band structure that is revealed by means of ARPES and DFT. Bismuth states mix with the topological surface states and bulk bands of IMTI dependently on the substrate composition, that is expected to affect the induced exchange interaction. By means of *ab initio* calculations we have shown how the exchange interaction produces splitting of 1D edge states in

the case of Bi nanoribbon, that makes this heterostructure promising for tunable and yet unobserved quantum Hall phases detection.

4. Methods

Intrinsic magnetic topological $MnBi_2Te_4$ compounds had been grown by Bridgeman method. Characterization of the $MnBi_2Te_4$-family monocrystals can be found in Refs. [1,17,58,59]. ARPES data were recorded using several facilities. Laboratory-based measurements were made using a SPECS GmbH ProvenX-ARPES system equipped with ASTRAIOS 190 electron energy analyzer with 2D-CMOS electron detector and a non-monochromated He Iα light source with hν=21.22 eV. ARPES spectra at various photon energies were measured at the BaDElPh beamline [76] of the Elettra synchrotron in Trieste and LOREA beamline of the ALBA synchrotron in Barcelona. All synchrotron measurements were carried out at $T = 17$ K using p-polarized photons.

Samples were cleaved *in situ* at the base pressure of 6×10^{-10} mbar. Crystal quality and surface cleanliness of the cleaved surfaces had been checked by low energy electron diffraction and XPS. Bismuth deposition has been done using standart Knudsen cell at the temperature of 700 K. The sample was held at room temperature during deposition, and had been annealed up to 500 K after film growth. Bi deposition rate has been checked by quartz microbalance. Additionally, the thickness of 1 BL of Bi has been verified by the procedure of XPS spectra fitting and analysis, ascribed in the manuscript, and double checked by means of comparison with Bi deposition on Bi_2Te_3 substrate.

Electronic structure calculations were carried out within the density functional theory using the projector augmented-wave (PAW) method [77] as implemented in the VASP code [78,79]. The exchange–correlation energy was treated using the generalized gradient approximation [80]. The Hamiltonian contained scalar relativistic corrections and the spin–orbit coupling was taken into account by the second variation method [81]. The crystal structure of $MnBi_2Te_4$ bulk was fully optimized to find the equilibrium lattice parameters and atomic positions. At that, a conjugate-gradient algorithm was used. In order to describe the van der Waals interactions we made use of the DFT-D3 approach with Becke-Johnson damping [82]. Spin–orbit coupling was always included when performing relaxations. The atomic coordinates were relaxed using a force tolerance criterion for convergence of 10^{-4} eV/Å and the convergence criterion for the total energy was 10^{-6} eV. The k-point meshes of 10×10×2 and 10×10×1 were used to sample the bulk and slab Brillouin zones, respectively. The Mn 3d-states were treated employing the GGA+U approach [83] within the Dudarev scheme [84]. The $U_{\text{eff}} = U - J$ value for the Mn 3d-states was chosen to be equal to 5.34 eV, as in previous works on $MnBi_2Te_4$ [1,17,58,62,63,71,72,75,85–87].

To simulate the Bi-bilayer on $MnBi_2Te_4$ surface a slab consisting of 6 septuple layers of $MnBi_2Te_4$ with optimized bulk lattice constant was used. The atomic positions of two Bi bilayers atoms (on the top and bottom sides of the slab) as well as topmost(lowest) SLs of the $MnBi_2Te_4$ slab were optimized. Substrate atoms of the central SLs were kept fixed at the bulk crystalline positions. The geometry optimization was performed until the residual force on atoms was smaller than 10 meV/Å.

To simulate the zig-zag edge of the Bi-bilayer we constructed the rectangular $1 \times 7\sqrt{3}$ $MnBi_2Te_4$ supercell the thickness of which was reduced to four SLs. Ontop of this supercell a Bi-bilayer ribbon of $\approx$ 41 Å width was placed. The distance between opposite edges of the ribbon in neighboring cells was about 10 Å. The atoms on the ribbon edges were relaxed up to the fifth atom from the edge.

CRediT authorship contribution statement

I.I. Klimovskikh: Writing – review & editing, Writing – original draft, Validation, Supervision, Project administration, Methodology, Investigation, Funding acquisition, Formal analysis, Data curation, Conceptualization. **S.V. Eremeev:** Writing – review & editing, Writing – original draft, Methodology, Investigation, Conceptualization. **D.A. Estyunin:** Writing – original draft, Investigation, Formal analysis. **S.O. Filnov:** Investigation, Formal analysis. **K. Shimada:** Investigation, Formal analysis. **V.A. Golyashov:** Investigation, Formal analysis. **N.Yu. Solovova:** Data curation, Formal analysis, Investigation. **O.E. Tereshchenko:** Investigation, Formal analysis. **K.A. Kokh:** Investigation, Formal analysis. **A.S. Frolov:** Methodology, Investigation, Formal analysis. **A.I. Sergeev:** Investigation, Formal analysis. **V.S. Stolyarov:** Investigation, Formal analysis. **V. Mikšić Trontl:** Investigation, Formal analysis. **L. Petaccia:** Methodology, Investigation, Formal analysis, Conceptualization. **G. Di Santo:** Methodology, Investigation, Formal analysis. **M. Tallarida:** Investigation, Formal analysis. **J. Dai:** Investigation, Formal analysis. **S. Blanco-Canosa:** Investigation, Formal analysis. **T. Valla:** Writing – original draft, Methodology, Investigation, Funding acquisition, Formal analysis. **A.M. Shikin:** Investigation, Formal analysis. **E.V. Chulkov:** Supervision, Project administration, Investigation.

Declaration of competing interest

The authors declare that they have no known competing financial interests or personal relationships that could have appeared to influence the work reported in this paper.

Data availability

Data will be made available on request.

Acknowledgments

I.I.K and T.V. acknowledge the support from the Red guipuzcoana de Ciencia, Tecnología e Innovación – Gipuzkoa NEXT 2023 from the Gipuzkoa Provincial Council. The project that gave rise to these results received the support of a fellowship from ”la Caixa” Foundation (ID 100010434). The fellowship code is LCF/BQ/PI24/12040021. The authors acknowledge support by Saint Petersburg State University, Russia (Grant No. ID 95442847). S.V.E. acknowledge support from the Government research assignment for ISPMS SB RAS, project FWRW-2022-0001 (in the part of the DFT calculations). The authors also acknowledge support by Russian Foundation for Basic Research (Grants No. 21-52-12024, and No. 19-29-12061) and state assignment of IGM SB RAS 122041400031-2. The calculations were partially performed using the equipment of the Shared Resource Center “Far Eastern Computing Resource” of IACP FEB RAS (https://cc.dvo.ru). S.B-C thanks the MINECO of Spain, project PID2021-122609NB-C21. A.S.F. and V.S.S. thank Russian Science Foundation, Grant No. 23-72-30004 (https://rscf.ru/project/23-72-30004/) and A.I.S. thanks Grant No. 23-72-00020 (https://rscf.ru/project/23-72-00020/) for supporting his work on synthesis. LOREA was co-funded by the European Regional Development Fund (ERDF) within the Framework of the Smart Growth Operative Programme 2014–2020. We acknowledge Luca Sancin and Jordi Prat for technical support during ARPES experiments at BaDElPh and LOREA beamlines, respectively. G.V.A. and O.E.T. acknowledge support from the SRF SKIF Boreskov Institute of Catalysis (FWUR-2024-0042).

Appendix A. Supplementary data

Supplementary material related to this article can be found online at https://doi.org/10.1016/j.mtadv.2024.100511.

References

[1] M.M. Otrokov, et al., Prediction and observation of an antiferromagnetic topological insulator, Nature 576 (2019) 416–422.

[2] T. Hirahara, et al., Large-gap magnetic topological heterostructure formed by subsurface incorporation of a ferromagnetic layer, Nano Lett. 17 (2017) 3493–3500.

[3] J. Wu, F. Liu, C. Liu, Y. Wang, C. Li, Y. Lu, S. Matsuishi, H. Hosono, Toward 2D magnets in the $(MnBi_2Te_4)(Bi_2Te_3)_n$ bulk crystal, Adv. Mater. 32 (2020) 2001815.

[4] D. Zhang, M. Shi, T. Zhu, D. Xing, H. Zhang, J. Wang, Topological axion states in the magnetic insulator $MnBi_2Te_4$ with the quantized magnetoelectric effect, Phys. Rev. Lett. 122 (2019) 206401.

[5] J. Li, Y. Li, S. Du, Z. Wang, B.-L. Gu, S.-C. Zhang, K. He, W. Duan, Y. Xu, Intrinsic magnetic topological insulators in van der Waals layered $MnBi_2Te_4$-family materials, Sci. Adv. 5 (2019) eaaw5685.

[6] Y. Gong, et al., Experimental realization of an intrinsic magnetic topological insulator, Chin. Phys. Lett. 36 (2019) 076801.

[7] S.H. Lee, et al., Spin scattering and noncollinear spin structure-induced intrinsic anomalous Hall effect in antiferromagnetic topological insulator $MnBi_2Te_4$, Phys. Rev. Res. 1 (2019) 012011.

[8] Z.S. Aliev, I.R. Amiraslanov, D.I. Nasonova, A.V. Shevelkov, N.A. Abdullayev, Z.A. Jahangirli, E.N. Orujlu, M.M. Otrokov, N.T. Mamedov, M.B. Babanly, E.V. Chulkov, Novel ternary layered manganese bismuth tellurides of the $MnTe$-Bi_2Te_3 system: Synthesis and crystal structure, J. Alloys Compd. 789 (2019) 443–450.

[9] Hao Y.-J. others, Gapless surface Dirac cone in antiferromagnetic topological insulator $MnBi_2Te_4$, Phys. Rev. X 9 (2019) 041038.

[10] Y.J. Chen, et al., Topological electronic structure and its temperature evolution in antiferromagnetic topological insulator $MnBi_2Te_4$, Phys. Rev. X 9 (2019) 041040.

[11] P. Swatek, Y. Wu, L.-L. Wang, K. Lee, B. Schrunk, J. Yan, A. Kaminski, Gapless Dirac surface states in the antiferromagnetic topological insulator $MnBi_2Te_4$, Phys. Rev. B 101 (2020) 161109.

[12] D.A. Estyunin, I.I. Klimovskikh, A.M. Shikin, E.F. Schwier, M.M. Otrokov, A. Kimura, S. Kumar, S.O. Filnov, Z.S. Aliev, M.B. Babanly, E.V. Chulkov, Signatures of temperature driven antiferromagnetic transition in the electronic structure of topological insulator $MnBi_2Te_4$, APL Mater. 8 (2020) 021105.

[13] X. Gui, I. Pletikosic, H. Cao, H.-J. Tien, X. Xu, R. Zhong, G. Wang, T.-R. Chang, S. Jia, T. Valla, W. Xie, R.J. Cava, A new magnetic topological quantum material candidate by design, ACS Central Sci. 5 (2019) 900–910.

[14] C.-Z. Chang, C.-X. Liu, A.H. MacDonald, Colloquium: Quantum anomalous Hall effect, Rev. Modern Phys. 95 (2023) 011002.

[15] P. Li, Prediction of intrinsic two dimensional ferromagnetism realized quantum anomalous Hall effect, Phys. Chem. Chem. Phys. 21 (2019) 6712–6717.

[16] K. Wang, Y. Li, H. Mei, P. Li, Z.-X. Guo, Quantum anomalous Hall and valley quantum anomalous Hall effects in two-dimensional d^0 orbital XY monolayers, Phys. Rev. Mater. 6 (2022) 044202.

[17] I.I. Klimovskikh, et al., Tunable 3D/2D magnetism in the $(MnBi_2Te_4)(Bi_2Te_3)_m$ topological insulators family, npj Quantum Mater. 5 (2020) 54.

[18] L. Rienks E. D., et al., Large magnetic gap at the Dirac point in $Bi_2Te_3/MnBi_2Te_4$ heterostructures, Nature 576 (2019) 423–428.

[19] Y. Deng, Y. Yu, M. Shi, et al., Quantum anomalous Hall effect in intrinsic magnetic topological insulator $MnBi_2Te_4$, Science 367 (2020) 895.

[20] J. Wang, B. Lian, H. Zhang, Y. Xu, S.-C. Zhang, Quantum anomalous Hall effect with higher plateaus, Phys. Rev. Lett. 111 (2013) 136801.

[21] M. Bosnar, A.Y. Vyazovskaya, E.K. Petrov, E.V. Chulkov, M.M. Otrokov, High Chern number van der Waals magnetic topological multilayers $MnBi_2Te_4$/h-BN, npj 2D Mater. Appl. 7 (2023) 33.

[22] P. Li, X. Li, W. Zhao, H. Chen, M.-X. Chen, Z.-X. Guo, J. Feng, X.-G. Gong, A.H. MacDonald, Topological Dirac states beyond π orbitals for silicene on SiC(0001) surface, Nano Lett. 17 (2017) 6195–6202, PMID: 28960082.

[23] H.P. Wang, W. Luo, H.J. Xiang, Prediction of high-temperature quantum anomalous Hall effect in two-dimensional transition-metal oxides, Phys. Rev. B 95 (2017) 125430.

[24] P. Li, X. Yang, Q.-S. Jiang, Y.-Z. Wu, W. Xun, Built-in electric field and strain tunable valley-related multiple topological phase transitions in $VSiXN_4 (X = C, Si, Ge, Sn, Pb)$ monolayers, Phys. Rev. Mater. 7 (2023) 064002.

[25] F. Xue, Y. Hou, Z. Wang, Z. Xu, K. He, R. Wu, Y. Xu, W. Duan, Tunable quantum anomalous Hall effects in ferromagnetic van der Waals heterostructures, Natl. Sci. Rev. 11 (2023) nwad151.

[26] Z. Li, J. Zhang, X. Hong, X. Feng, Y. Xu, K. He, 2024. arXiv:2401.08490.

[27] K. Shen, C. Hua, Z. Liang, Y. Wang, H. Sun, J. Hu, H. Zhang, H. Li, Z. Jiang, H. Huang, P. Wang, Z. Sun, E. Wahlström, Y. Lu, F. Song, Epitaxial growth of free-standing bismuth film on graphene embedded with nontrivial properties, ACS Appl. Electron. Mater. 1 (2019) 1817–1824.

[28] H.W. Yeom, K.-H. Jin, S.-H. Jhi, Topological fate of edge states of single Bi bilayer on Bi(111), Phys. Rev. B 93 (2016) 075435.

[29] Z. Li, Z. Zhang, Tuning the topological bandgap of bilayer-Bi(111) supported on graphene, Physica Status Solidi (RRL) 14 (2020) 2000131.

[30] F. Reis, G. Li, L. Dudy, M. Bauernfeind, S. Glass, W. Hanke, R. Thomale, J. Schäfer, R. Claessen, Bismuthene on a SiC substrate: A candidate for a high-temperature quantum spin Hall material, Science 357 (2017) 287–290.

[31] G. Bian, Z. Wang, X.-X. Wang, C. Xu, S. Xu, T. Miller, M.Z. Hasan, F. Liu, T.-C. Chiang, Engineering electronic structure of a two-dimensional topological insulator Bi(111) bilayer on Sb nanofilms by quantum confinement effect, ACS Nano 10 (2016) 3859–3864.

[32] H.-H. Sun, M.-X. Wang, F. Zhu, G.-Y. Wang, H.-Y. Ma, Z.-A. Xu, Q. Liao, Y. Lu, C.-L. Gao, Y.-Y. Li, C. Liu, D. Qian, D. Guan, J.-F. Jia, Coexistence of topological edge state and superconductivity in bismuth ultrathin film, Nano Lett. 17 (2017) 3035–3039.

[33] J. Gou, L. Kong, X. He, Y.L. Huang, J. Sun, S. Meng, K. Wu, L. Chen, A.T.S. Wee, The effect of moire superstructures on topological edge states in twisted bismuthene homojunctions, Sci. Adv. 6 (2020) eaba2773.

[34] J. Gou, H. Bai, X. Zhang, Y.L. Huang, S. Duan, A. Ariando, S.A. Yang, L. Chen, Y. Lu, A.T.S. Wee, Two-dimensional ferroelectricity in a single-element bismuth monolayer, Nature 617 (2023) 67–72.

[35] P. Li, C. Wu, C. Peng, M. Yang, W. Xun, Multifield tunable valley splitting in two-dimensional MXene Cr_2COOH, Phys. Rev. B 108 (2023) 195424.

[36] W. Xun, C. Wu, H. Sun, W. Zhang, Y.-Z. Wu, P. Li, Coexisting magnetism, ferroelectric, and ferrovalley multiferroic in stacking-dependent two-dimensional materials, Nano Lett. 24 (2024) 3541–3547, PMID: 38451854.

[37] L. Peng, J.-J. Xian, P. Tang, A. Rubio, S.-C. Zhang, W. Zhang, Y.-S. Fu, Visualizing topological edge states of single and double bilayer Bi supported on multibilayer Bi(111) films, Phys. Rev. B 98 (2018) 245108.

[38] I.K. Drozdov, A. Alexandradinata, S. Jeon, S. Nadj-Perge, H. Ji, R.J. Cava, B. Andrei Bernevig, A. Yazdani, One-dimensional topological edge states of bismuth bilayers, Nat. Phys. 10 (2014) 664–669.

[39] S.H. Kim, K.-H. Jin, J. Park, J.S. Kim, S.-H. Jhi, T.-H. Kim, H.W. Yeom, Edge and interfacial states in a two-dimensional topological insulator: Bi(111) bilayer on Bi_2Te_2Se, Phys. Rev. B 89 (2014) 155436.

[40] H.W. Yeom, S.H. Kim, W.J. Shin, K.-H. Jin, J. Park, T.-H. Kim, J.S. Kim, H. Ishikawa, K. Sakamoto, S.-H. Jhi, Transforming a surface state of a topological insulator by a Bi capping layer, Phys. Rev. B 90 (2014) 235401.

[41] T. Hirahara, G. Bihlmayer, Y. Sakamoto, M. Yamada, H. Miyazaki, Kimura, S. Blügel, S. Hasegawa, Interfacing 2D and 3D topological insulators: Bi(111) bilayer on Bi_2Te_3, Phys. Rev. Lett. 107 (2011) 166801.

[42] C. Niu, G. Bihlmayer, H. Zhang, D. Wortmann, S. Blügel, Y. Mokrousov, Functionalized bismuth films: Giant gap quantum spin Hall and valley-polarized quantum anomalous Hall states, Phys. Rev. B 91 (2015) 041303.

[43] K.-H. Jin, S.-H. Jhi, Quantum anomalous Hall and quantum spin-Hall phases in flattened Bi and Sb bilayers, Sci. Rep. 5 (2015) 8426.

[44] Y. Yang, Z. Xu, L. Sheng, B. Wang, D.Y. Xing, D.N. Sheng, Time-reversal-symmetry-broken quantum spin Hall effect, Phys. Rev. Lett. 107 (2011) 066602.

[45] H. Zhang, F. Freimuth, G. Bihlmayer, S. Blügel, Y. Mokrousov, Topological phases of Bi(111) bilayer in an external exchange field, Phys. Rev. B 86 (2012) 035104.

[46] I.I. Naumov, P. Dev, Coexistence of quantum spin Hall and magnetic states in zigzag bismuth nanoribbons, Appl. Phys. Lett. 123 (2023) 093104.

[47] L. Miao, et al., Quasiparticle dynamics in reshaped helical Dirac cone of topological insulators, Proc. Natl. Acad. Sci. 110 (2013) 2758–2762.

[48] L. Miao, Z.F. Wang, M.-Y. Yao, F. Zhu, J.H. Dil, C.L. Gao, C. Liu, F. Liu, D. Qian, J.-F. Jia, Orbit- and atom-resolved spin textures of intrinsic, extrinsic, and hybridized Dirac cone states, Phys. Rev. B 89 (2014) 155116.

[49] P. Zhang, P. Richard, T. Qian, Y.-M. Xu, X. Dai, H. Ding, A precise method for visualizing dispersive features in image plots, Rev. Sci. Instrum. 82 (2011) 043712.

[50] H. Li, S. Liu, C. Liu, J. Zhang, Y. Xu, R. Yu, Y. Wu, Y. Zhang, S. Fan, Antiferromagnetic topological insulator $MnBi_2Te_4$: Synthesis and magnetic properties, Phys. Chem. Chem. Phys. 22 (2020) 556–563.

[51] T. Makarova, D. Estyunin, S. Filnov, et al., Impact of Co atoms on the electronic structure of Bi_2Te_3 and $MnBi_2Te_4$ topological insulators, JETP 134 (2021) 607.

[52] D.A. Estyunin, T.P. Makarova, K.A. Kokh, O.E. Tereshchenko, A.M. Shikin, I.I. Klimovskikh, Contact of the intrinsic magnetic topological insulator $Mn(Bi, Sb)_2Te_4$ with a superconducting Pb film, Phys. Rev. B 106 (2022) 155305.

[53] I.I. Klimovskikh, D.A. Estyunin, T.P. Makarova, O.E. Tereshchenko, K.A. Kokh, A.M. Shikin, Electronic structure of Pb adsorbed surfaces of intrinsic magnetic topological insulators, J. Phys. Chem. Lett. 13 (2022) 6628–6634.

[54] T. Valla, H. Ji, L.M. Schoop, A.P. Weber, Z.-H. Pan, J.T. Sadowski, E. Vescovo, A.V. Fedorov, A.N. Caruso, Q.D. Gibson, L. Müchler, C. Felser, R.J. Cava, Topological semimetal in a Bi-Bi_2Se_3 infinitely adaptive superlattice phase, Phys. Rev. B 86 (2012) 241101.

[55] Q.D. Gibson, L.M. Schoop, A.P. Weber, H. Ji, S. Nadj-Perge, I.K. Drozdov, H. Beidenkopf, J.T. Sadowski, A. Fedorov, A. Yazdani, T. Valla, R.J. Cava, Termination-dependent topological surface states of the natural superlattice phase Bi_4Se_3, Phys. Rev. B 88 (2013) 081108.

[56] I.I. Klimovskikh, D. Sostina, A. Petukhov, A.G. Rybkin, S.V. Eremeev, E.V. Chulkov, O.E. Tereshchenko, K.A. Kokh, A.M. Shikin, Spin-resolved band structure of heterojunction Bi-bilayer/3D topological insulator in the quantum dimension regime in annealed $Bi_2Te_{2.4}Se_{0.6}$, Sci. Rep. 7 (2017) 45797.

[57] R.C. Vidal, et al., Surface states and rashba-type spin polarization in antiferromagnetic $MnBi_2Te_4$(0001), Phys. Rev. B 100 (2019) 121104.

[58] A.M. Shikin, et al., Sample-dependent Dirac-point gap in $MnBi_2Te_4$ and its response to applied surface charge: A combined photoemission and ab initio study, Phys. Rev. B 104 (2021) 115168.

[59] A.S. Frolov, et al., Magnetic Dirac semimetal state of (Mn, Ge)Bi2Te4, Commun. Phys. 7 (2024) 180.

[60] T.P. Estyunina, A.M. Shikin, D.A. Estyunin, A.V. Eryzhenkov, I.I. Klimovskikh, K.A. Bokai, V.A. Golyashov, K.A. Kokh, O.E. Tereshchenko, S. Kumar, K. Shimada, A.V. Tarasov, Evolution of $Mn_{1-x}Ge_xBi_2Te_4$ electronic structure under variation of Ge content, Nanomaterials (2023) 13.

[61] D.A. Estyunin, A.A. Rybkina, K.A. Kokh, O.E. Tereshchenko, M.V. Likholetova, I.I. Klimovskikh, A.M. Shikin, Comparative study of magnetic properties of $(Mn_{1-x}A^{IV}_x)Bi_2Te_4A^{IV}$, Sn, Magnetochemistry 0 (2023) 9.

[62] M.M. Otrokov, I.P. Rusinov, M. Blanco-Rey, M. Hoffmann, A.Y. Vyazovskaya, S.V. Eremeev, A. Ernst, P.M. Echenique, A. Arnau, E.V. Chulkov, Unique thickness-dependent properties of the van der Waals interlayer antiferromagnet $MnBi_2Te_4$ films, Phys. Rev. Lett. 122 (2019) 107202.

[63] S.V. Eremeev, M.M. Otrokov, E.V. Chulkov, Competing rhombohedral and monoclinic crystal structures in $MnPn_2Ch_4$ compounds: An ab-initio study, J. Alloys Compd. 709 (2017) 172–178.

[64] R. Dronskowski, P.E. Bloechl, Crystal orbital Hamilton populations (COHP): Energy-resolved visualization of chemical bonding in solids based on density-functional calculations, J. Phys. Chem. 97 (1993) 8617–8624.

[65] V.L. Deringer, A.L. Tchougréeff, R. Dronskowski, Crystal Orbital Hamilton Population (COHP) analysis as projected from plane-wave basis sets, J. Phys. Chem. A 115 (2011) 5461–5466.

[66] S. Maintz, V.L. Deringer, A.L. Tchougréeff, R. Dronskowski, LOBSTER: A tool to extract chemical bonding from plane-wave based DFT, J. Comput. Chem. 37 (2016) 1030–1035.

[67] V.N. Men'shov, V.V. Tugushev, T.V. Menshchikova, S.V. Eremeev, P.M. Echenique, E.V. Chulkov, Modelling near-surface bound electron states in a 3D topological insulator: Analytical and numerical approaches, J. Phys.: Condens. Matter. 26 (2014) 485003.

[68] S.V. Eremeev, S.S. Tsirkin, I.A. Nechaev, P.M. Echenique, E.V. Chulkov, New generation of two-dimensional spintronic systems realized by coupling of Rashba and Dirac fermions, Sci. Rep. 5 (2015) 12819.

[69] O. De Luca, I.A. Shvets, S.V. Eremeev, Z.S. Aliev, M. Kopciuszynski, A. Barinov, F. Ronci, S. Colonna, E.V. Chulkov, R.G. Agostino, M. Papagno, R. Flammini, Floating of the topological surface state on top of a thick lead layer: The case of the Pb/Bi_2Se_3 interface, Phys. Rev. Mater. 7 (2023) 124203.

[70] N.L. Zaitsev, I.P. Rusinov, T.V. Menshchikova, E.V. Chulkov, Interplay between exchange-split Dirac and rashba-type surface states at the $MnBi_2Te_4$/BiTeI interface, Phys. Rev. B 107 (2023) 045402.

[71] M.M. Otrokov, T.V. Menshchikova, I.P. Rusinov, M.G. Vergniory, V.M. Kuznetsov, E.V. Chulkov, Magnetic extension as an efficient method for realizing the quantum anomalous Hall state in topological insulators, JETP Lett. 105 (2017) 297–302.

[72] M.M. Otrokov, T.V. Menshchikova, M.G. Vergniory, I.P. Rusinov, A.Y. Vyazovskaya, Y.M. Koroteev, G. Bihlmayer, A. Ernst, P.M. Echenique, A. Arnau, E.V. Chulkov, Highly-ordered wide bandgap materials for quantized anomalous Hall and magnetoelectric effects, 2D Mater. 4 (2017) 025082.

[73] M. Wada, S. Murakami, F. Freimuth, G. Bihlmayer, Localized edge states in two-dimensional topological insulators: Ultrathin Bi films, Phys. Rev. B 83 (2011) 121310.

[74] P.M. Sass, W. Ge, J. Yan, D. Obeysekera, J.J. Yang, W. Wu, Magnetic imaging of domain walls in the antiferromagnetic topological insulator $MnBi_2Te_4$, Nano Lett. 20 (2020) 2609–2614.

[75] M. Garnica, et al., Native point defects and their implications for the Dirac point gap at $MnBi_2Te_4(0001)$, npj Quantum Mater. 7 (2022) 7.

[76] L. Petaccia, P. Vilmercati, S. Gorovikov, M. Barnaba, A. Bianco, D. Cocco, C. Masciovecchio, A. Goldoni, BaD ElPh: A 4 m normal-incidence monochromator beamline at Elettra, Nucl. Instrum. Methods Phys. Res. A 606 (2009) 780–784.

[77] P.E. Blöchl, Projector augmented-wave method, Phys. Rev. B 50 (1994) 17953–17979.

[78] G. Kresse, J. Furthmüller, Efficient iterative schemes for ab initio total-energy calculations using a plane-wave basis set, Phys. Rev. B 54 (1996) 11169–11186.

[79] G. Kresse, D. Joubert, From ultrasoft pseudopotentials to the projector augmented-wave method, Phys. Rev. B 59 (1999) 1758–1775.

[80] J.P. Perdew, K. Burke, M. Ernzerhof, Generalized gradient approximation made simple, Phys. Rev. Lett. 77 (1996) 3865–3868.

[81] D.D. Koelling, B.N. Harmon, A technique for relativistic spin-polarised calculations, J. Phys. C: Sol. St. Phys. 10 (1977) 3107.

[82] S. Grimme, S. Ehrlich, L. Goerigk, Effect of the damping function in dispersion corrected density functional theory, J. Comput. Chem. 32 (2011) 1456–1465.

[83] V.I. Anisimov, J. Zaanen, O.K. Andersen, Band theory and mott insulators: Hubbard U instead of Stoner I, Phys. Rev. B 44 (1991) 943–954.

[84] S.L. Dudarev, G.A. Botton, S.Y. Savrasov, C.J. Humphreys, A.P. Sutton, Electron-energy-loss spectra and the structural stability of nickel oxide: An LSDA+U study, Phys. Rev. B 57 (1998) 1505–1509.

[85] S.V. Eremeev, M.M. Otrokov, E.V. Chulkov, New universal type of interface in the magnetic insulator/topological insulator heterostructures, Nano Lett. 18 (2018) 6521–6529.

[86] T. Hirahara, et al., Fabrication of a novel magnetic topological heterostructure and temperature evolution of its massive Dirac cone, Nature Commun. 11 (2020) 4821.

[87] A.M. Shikin, et al., Nature of the Dirac gap modulation and surface magnetic interaction in axion antiferromagnetic topological insulator $MnBi_2Te_4$, Sci. Rep. 10 (2020) 13226.